


Anisotropic variational models and PDEs for inverse imaging problems

PhD Candidate: Simone Parisotto[1]
Supervisor: Prof. Carola-Bibiane Schönlieb[2] - Co-supervisor: Prof. Simon Masnou[3]

[1] Cambridge Centre for Analysis, University of Cambridge, United Kingdom
[2] DAMTP, University of Cambridge, United Kingdom
[3] Institut Camille Jordan, Université Lyon 1, France

PhD defense - Cambridge, 8th February 2019

Topics of my research

Higher-order total directional variation (for images and videos)

Anisotropic generalisation of osmosis filter (for shadow removal)

Mathematics for CH (for frescoes and manuscripts restoration)

TDV: theoretical motivation

Total generalized variation (Bredies, Holler, Kunisch, Pock, 2010-present)

$$\mathrm{TGV}^{q,\ell}_{\boldsymbol{\alpha}}(\boldsymbol{u}) = \sup_{\boldsymbol{\Psi}} \left\{ \int_\Omega \boldsymbol{u} \cdot \mathrm{div}^q\, \boldsymbol{\Psi}\, \mathrm{d}\boldsymbol{x},\ \text{for all } \boldsymbol{\Psi} \in \mathcal{Y}^{q,\ell}_{\boldsymbol{\alpha}} \right\},\ \text{with } \boldsymbol{\alpha} \text{ positive weights},$$

$$\mathcal{Y}^{q,\ell}_{\boldsymbol{\alpha}} := \left\{ \boldsymbol{\Psi} \,:\, \boldsymbol{\Psi} \in \mathrm{C}^q_c(\Omega, \mathrm{Sym}^{\ell+q}(\mathbb{R}^d)),\ \left\|\mathrm{div}^j\, \boldsymbol{\Psi}\right\|_\infty \leq \alpha_j,\ j = 0, \dots, q-1 \right\}.$$

Proposed: (higher-order) directional generalization

Let also a collection of weighting fields $\mathcal{M} = (\mathbf{M}_j)_{j=1}^q$ with $\mathbf{M}_j \in \mathrm{C}^\infty(\Omega, \mathcal{T}^2(\mathbb{R}^d))$:

$$\mathrm{TDV}^{q,\ell}_{\boldsymbol{\alpha}}(\boldsymbol{u}, \mathcal{M}) = \sup_{\boldsymbol{\Psi}} \left\{ \int_\Omega \boldsymbol{u} \cdot \mathrm{div}^q_{\mathcal{M}}\, \boldsymbol{\Psi}\, \mathrm{d}\boldsymbol{x},\ \text{for all } \boldsymbol{\Psi} \in \mathcal{Y}^{q,\ell}_{\mathcal{M},\boldsymbol{\alpha}} \right\},$$

$$\mathcal{Y}^{q,\ell}_{\mathcal{M},\boldsymbol{\alpha}} := \left\{ \boldsymbol{\Psi} \,:\, \boldsymbol{\Psi} \in \mathrm{C}^q_c(\Omega, \mathcal{T}^{\ell+q}(\mathbb{R}^d)),\ \left\|\mathrm{div}^j_{\mathcal{M}}\, \boldsymbol{\Psi}\right\|_\infty \leq \alpha_j,\ j = 0, \dots, q-1 \right\},$$

$$\mathrm{div}^0_{\mathcal{M}}\, \boldsymbol{\Psi} := \boldsymbol{\Psi}, \quad \mathrm{div}^j_{\mathcal{M}}(\boldsymbol{\Psi}) := \mathrm{div}_{\mathbf{M}_{q-j+1}} \left(\mathrm{div}^{j-1}_{\mathcal{M}}\, \boldsymbol{\Psi} \right).$$

- if $\mathcal{M} = (\mathbf{I})_{j=1}^q$ then $\mathrm{TDV}^{q,\ell}_{\boldsymbol{\alpha}}(\boldsymbol{u}, \mathcal{M}) \equiv \neg\mathrm{symTGV}^{q,\ell}_{\boldsymbol{\alpha}}(u)$;
- if $\boldsymbol{\Psi} \in \mathrm{C}^q_c(\Omega, \mathrm{Sym}^{\ell+q}(\mathbb{R}^d))$ and $\mathcal{M} = (\mathbf{I})_{j=1}^q$ then $\mathrm{TDV}^{q,\ell}_{\boldsymbol{\alpha}}(\boldsymbol{u}, \mathcal{M}) \equiv \mathrm{TGV}^{q,\ell}_{\boldsymbol{\alpha}}(u)$;
- it extends also the work of (Kongskov and Dong, 2017).

TDV: motivation for imaging applications

For $q = 1$, $\ell = 0$: weak: $\displaystyle\int_\Omega u \cdot \operatorname{div}_{\mathbf{M}} \boldsymbol{\Psi}\, \mathrm{d}\boldsymbol{x}$ strong: $\displaystyle\int_\Omega (\mathbf{M}\,\boldsymbol{\nabla} \otimes u) \cdot \boldsymbol{\Psi}\, \mathrm{d}\boldsymbol{x}$

$$(\mathbf{M}\,\boldsymbol{\nabla} \otimes u) = \underbrace{\begin{pmatrix} b_1 & 0 \\ 0 & b_2 \end{pmatrix} \begin{pmatrix} \cos\boldsymbol{\theta} & \sin\boldsymbol{\theta} \\ -\sin\boldsymbol{\theta} & \cos\boldsymbol{\theta} \end{pmatrix}}_{\mathbf{M}=\Lambda_{\boldsymbol{b}} R_{\boldsymbol{\theta}}^{\mathrm{T}}} \begin{pmatrix} \partial_x u \\ \partial_y u \end{pmatrix} = \begin{pmatrix} b_1\, \boldsymbol{\nabla}_{\boldsymbol{v}}\, u \\ b_2\, \boldsymbol{\nabla}_{\boldsymbol{v}^\perp}\, u \end{pmatrix}, \text{ with } \boldsymbol{v} = (\cos\boldsymbol{\theta}, \sin\boldsymbol{\theta}).$$

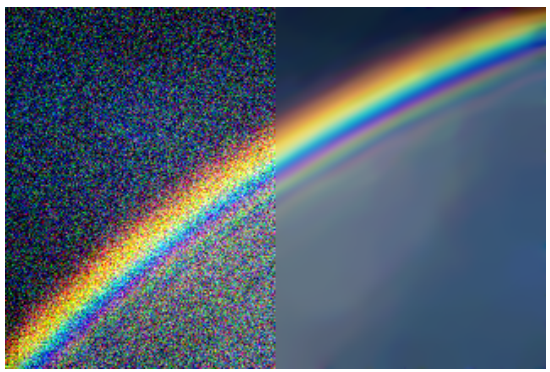

Denoising (20% G. noise)

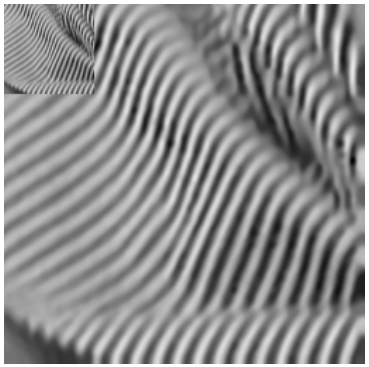

4X Wavelet zooming

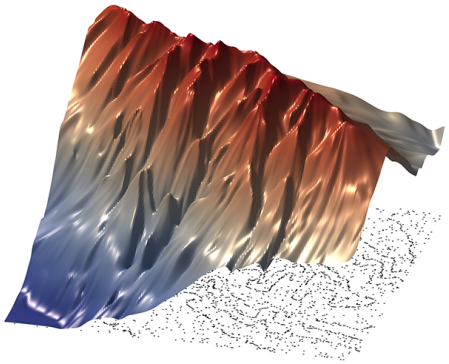

DEM interp. (7% data)

Adjoint: $$\int_\Omega (\mathbf{M}\,\boldsymbol{\nabla} \otimes \boldsymbol{u}) \cdot \boldsymbol{\Psi}\, \mathrm{d}\boldsymbol{x} = -\int_\Omega \boldsymbol{u} \cdot \underbrace{\operatorname{trace}\left(\boldsymbol{\nabla} \otimes [\operatorname{trace}\left(\mathbf{M} \otimes \boldsymbol{\Psi}^{\sim}\right)]^{\sim}\right)}_{\operatorname{div}_{\mathbf{M}} \boldsymbol{\Psi}} \mathrm{d}\boldsymbol{x}.$$

TDV: more theory

TDV as Radon norm for general q

$$\mathrm{TDV}^{q,\ell}(\boldsymbol{u}, \mathcal{M}) = \|\mathbf{M}_q \boldsymbol{\nabla} \otimes \cdots \otimes \mathbf{M}_1 \boldsymbol{\nabla} \otimes \boldsymbol{u}\|_{\mathscr{M}(\Omega, \mathcal{T}^{\ell+q}(\mathbb{R}^d))},$$

$$\mathrm{BDV}^q(\Omega, \mathcal{M}, \mathcal{T}^\ell(\mathbb{R}^d)) = \left\{ \boldsymbol{u} \in \mathrm{L}^1(\Omega, \mathcal{T}^\ell(\mathbb{R}^d)) \,\middle|\, \mathrm{TDV}^{q,\ell}_{\boldsymbol{\alpha}}(\boldsymbol{u}, \mathcal{M}) < \infty \right\}.$$

- the spaces are nested: the larger is q, the smaller is the space;
- BDV^q is a Banach space with $\|\boldsymbol{u}\|_1 + \|\mathbf{M}_q \boldsymbol{\nabla} \otimes \cdots \otimes \mathbf{M}_1 \boldsymbol{\nabla} \otimes \boldsymbol{u}\|_{\mathscr{M}}$;
- $\mathrm{TDV}^{q,\ell}_{\boldsymbol{\alpha}}$ is convex and lower semi-continuous.

By adapting the work of Bredies and Holler (2014):

Theorem: existence of TDV-regularised solutions

Let $p \in [1, \infty]$ with $p \leq d/(d-1)$ and assume that $F : \mathrm{L}^p(\Omega, \mathcal{T}^\ell(\mathbb{R}^d)) \to]-\infty, +\infty]$ is proper, convex, lower semi-continuous and coercive. Then there exist a solution of

$$\min_{\boldsymbol{u} \in \mathrm{L}^p(\Omega, \mathcal{T}^\ell(\mathbb{R}^d))} \mathrm{TDV}^{q,\ell}_{\boldsymbol{\alpha}}(\boldsymbol{u}, \mathcal{M}) + F(\boldsymbol{u}).$$

In general **uniqueness** does not hold since $\mathrm{TDV}^{q,\ell}_{\boldsymbol{\alpha}}$ is not strictly convex.

TDV: continuous regularisation problem

Single continuous problem ($q \in \mathbb{N}$ fixed)

$$u^\star = \operatorname*{arg\,min}_{u \in \mathbb{R}^{|\Omega|}} \mathrm{TDV}^{q,0}_{\boldsymbol{\alpha}_q}(u, \mathcal{M}_q) + \frac{\eta}{2} \left\| \mathcal{S}u - u^\diamond \right\|_2^2 .$$

Joint continuous problem ($\mathrm{Q} \in \mathbb{N}$ fixed)

$$u^\star = \operatorname*{arg\,min}_{u \in \mathbb{R}} \sum_{q=1}^{\mathrm{Q}} \mathrm{TDV}^{q,0}_{\boldsymbol{\alpha}_q}(u, \mathcal{M}_q) + \frac{\eta}{2} \left\| \mathcal{S}u - u^\diamond \right\|_2^2 .$$

Equivalent decomposition in terms of iterated Fenchel duality

Similar to TGV (Bredies & Holler, 2014), now with $\mathbf{M}_{q,j}\, \boldsymbol{\nabla}$ instead of $\mathcal{E}$ (symm. gradient):

$$\mathrm{TDV}^{q,\ell}_{\boldsymbol{\alpha}_q}(u, \mathcal{M}_q) = \inf_{\substack{u_j \in \mathrm{BDV}^{q-j}(\Omega, \mathbf{M}_{q,j+1}, \mathcal{T}^{\ell+j}(\mathbb{R}^d)) \\ j=1,\dots,q-1, u_0 = u,\, u_q = 0}} \left(\sum_{j=1}^{q} \alpha_{q,q-j} \left\| \mathbf{M}_{q,j}\, \boldsymbol{\nabla}\, u_{j-1} - u_j \right\|_1 \right) .$$

TDV: discrete regularisation problem

Equivalent discrete decomposition in terms of iterated Fenchel duality

$$\mathrm{TDV}^{q,h}_{\boldsymbol{\alpha}_q}(u^h, \mathcal{M}^h_q) = \inf_{\substack{\boldsymbol{z}^h_j \in \mathrm{X}^{j,h}_\iota \\ j=0,\dots,q, \\ \boldsymbol{z}^h_0 = u^h,\, \boldsymbol{z}^h_q = 0}} \sum_{j=1}^{q} \alpha_{q,q-j} \left\| (\mathcal{K}^h_q)_{j,j} \boldsymbol{z}^h_{j-1} - \boldsymbol{z}^h_j \right\|_{2,1},$$

$$\text{with } (\mathcal{K}^h_q)_{j,j} = \begin{cases} (\mathcal{W}^j)^{\mathrm{T}} \mathbf{M}^h_{q,j} \mathcal{W}^j \boldsymbol{\nabla}^h & \text{if } j = 1, \dots q-1, \\ \mathbf{M}^h_{q,q} \mathcal{W}^q \boldsymbol{\nabla}^h & \text{if } j = q. \end{cases}$$

Joint discrete problem ($\mathrm{Q} \in \mathbb{N}$ fixed) and saddle-point problem (by duality of $\|\cdot\|_{2,1}$)

$$u^\star = \operatorname*{arg\,min}_{u^h \in \mathbb{R}^{|\Omega^h|}} \inf_{\boldsymbol{z}^h} \sum_{q=1}^{\mathrm{Q}} \underbrace{\sum_{j=1}^{q} \mathbf{A}_{j,q} \left\| \sum_{\ell=1}^{q} (\mathcal{K}^h_q)_{j,\ell} \boldsymbol{z}^h_{\ell-1} \right\|_{2,1}}_{\mathrm{TDV}^{q,h}_{\boldsymbol{\alpha}_q}(u^h, \mathcal{M}^h_q)} + \frac{\eta}{2} \left\| \mathcal{S} u^h - u^{\diamond,h} \right\|_2^2,$$

leading (and solved via primal-dual algorithm (Chambolle & Pock, 2011)) to:

$$\min_{\boldsymbol{z}^h} \max_{\boldsymbol{w}^h} \sum_{q=1}^{\mathrm{Q}} \langle \sum_{\ell=1}^{q} (\mathcal{K}^h_q)_{j,\ell} \boldsymbol{z}^h_{\ell-1}, \boldsymbol{w}^h_{q,j} \rangle - \underbrace{\sum_{q=1}^{\mathrm{Q}} \sum_{j=1}^{q} \delta_{\left\{ \|\cdot\|_{2,\infty} \le \mathbf{A}_{j,q} \right\}}(\boldsymbol{w}^h_{q,j})}_{F^*(\boldsymbol{w}^h)} + \underbrace{\frac{\eta}{2} \left\| \mathcal{S} \boldsymbol{z}^h_0 - \boldsymbol{z}^{\diamond,h}_0 \right\|_2^2}_{G(\boldsymbol{z}^h_0)}.$$

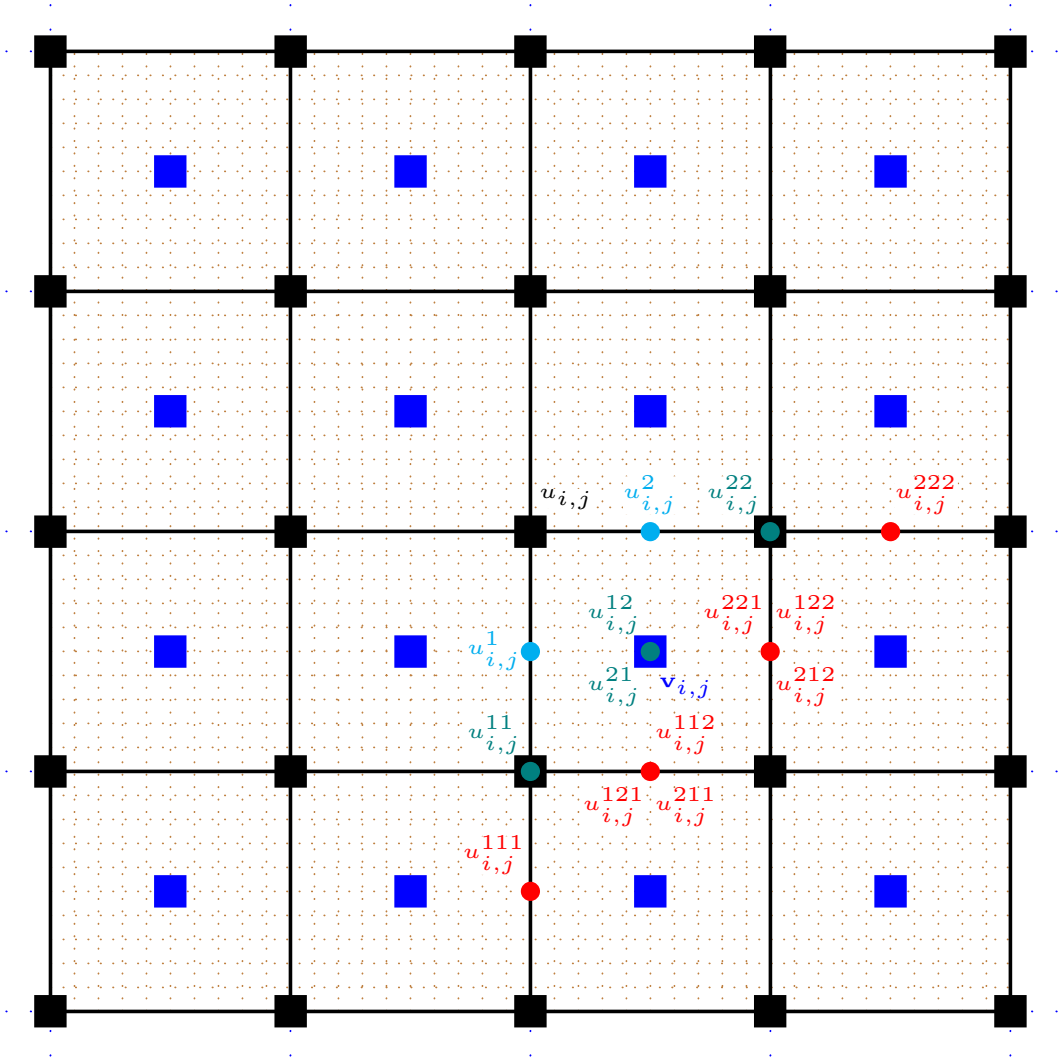

Staggered Grids. $u^h \in \mathbb{R}^{|\Omega^h|}$ (■), $\boldsymbol{v}^h \in \Gamma^h$ (■), $\boldsymbol{\nabla}^h u$ (●), $\boldsymbol{\nabla}^{2,h} u$ (●), $\boldsymbol{\nabla}^{3,h} u$ (●).

For $\mathbf{M}\,\boldsymbol{\nabla} \otimes u$ we need transfer operators $\mathcal{W}$ to match (●, ●, ●) with (■) and vice-versa.

TDV: image denoising

Original u

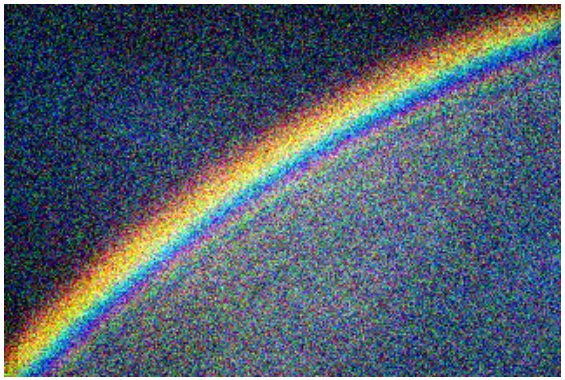

Noisy u (20% Gaussian)

BM3D
PSNR = 34.53

$b_2(\boldsymbol{x})$ in $\boldsymbol{b} = (1, b_2(\boldsymbol{x}))$ for M
$(\sigma, \rho) = (2, 30)$

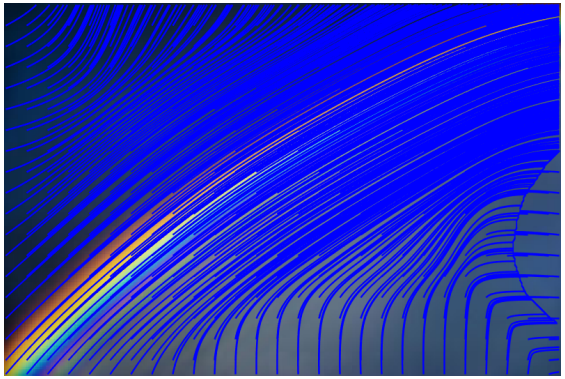

$\boldsymbol{v} = \boldsymbol{e}_1$ in Structure Tensor for M
$(\sigma, \rho) = (2, 30)$

Our, joint 1st and 3rd.
$\eta = 3.5$, $\boldsymbol{v}$, $\boldsymbol{b} = (1, b_2(\boldsymbol{x}))$
PSNR = 35.91

Rainbow image (320×214 pixels, photo by M.P. Markkanen, CC-BY-SA-4.0 license).

TDV: Digital Elevation Maps

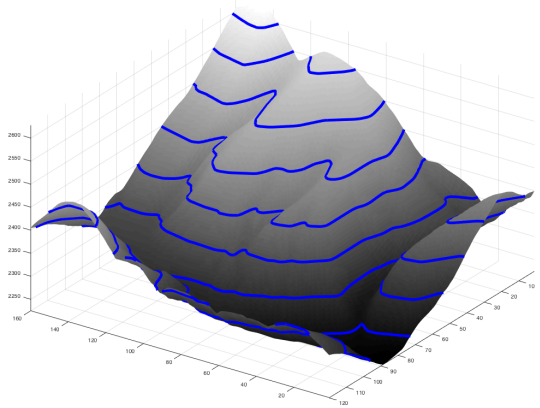

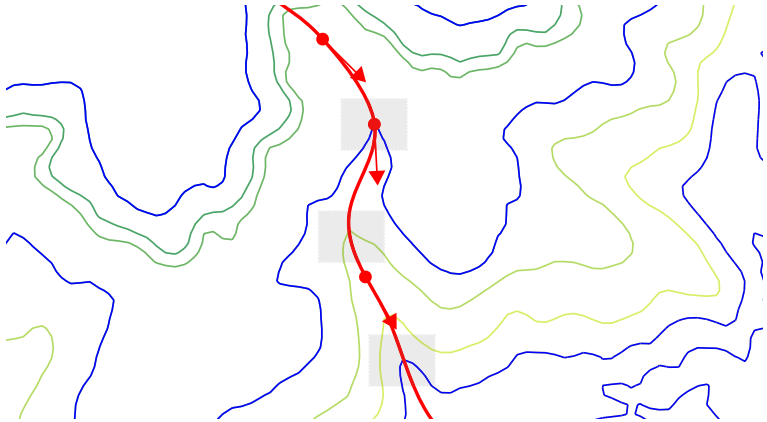

Find a naturally looking dense surface u that fits contour lines (partially given)

- u should coincide with the given sparse height values u_0;
- u should preserve the geometry (cusps, kinks) of the given level lines;
- u should be *smooth only* across level lines.

In [Lellmann, Morel & Schönlieb (2013)], alternatingly solved (CVX, variable size limit):

$$u^* = \arg\min_u \int_\Omega \left\| \nabla_{\boldsymbol{v}} (\nabla^2 u) \right\|_2 \mathrm{d}\boldsymbol{x} + \text{data constraint};$$

$$\widetilde{\boldsymbol{v}} = \arg\min_{\boldsymbol{y},\, \|\boldsymbol{y}\|_2 = 1} \left\| K_\sigma * \nabla \left(\frac{\nabla u}{|\nabla u|} \right) (\boldsymbol{x})\, \boldsymbol{y} \right\|_2 + \text{find } \boldsymbol{v} \text{ by a further regularization step.}$$

Surface interpolation. Find u, v via alternating minimisation.

$$u^\star = \arg\min_u \sum_{q=1}^{\mathrm{Q}} \mathrm{TDV}^q_{\boldsymbol{\alpha}_q}(u, \mathcal{M}_q(\boldsymbol{v})) + \frac{\eta}{2} \|\mathcal{S}u - u^\diamond\|_2^2 ,$$

$$\boldsymbol{v}^\star = \arg\min_{\boldsymbol{v}} \mu \mathrm{TV}(\boldsymbol{v}) + \zeta \int_\Omega \left(1 - \boldsymbol{v} \cdot \frac{\boldsymbol{\nabla} u}{|\boldsymbol{\nabla} u|}\right)^2 \mathrm{d}\boldsymbol{x}.$$

- $\mathcal{M}_q(\boldsymbol{v}) = (\mathbf{I}, \ldots, \mathbf{I}, \mathbf{M}(\boldsymbol{v}))$, with $\mathbf{M}(\boldsymbol{v}) := \Lambda_{\boldsymbol{b}} R^{\mathrm{T}}_{\boldsymbol{\theta}}$;
- $\mathcal{S}$ is a projection operator (leading to non accelerated primal-dual);
- the fidelity term in the second problem echoes the one in [Ballester et al. (2001)].

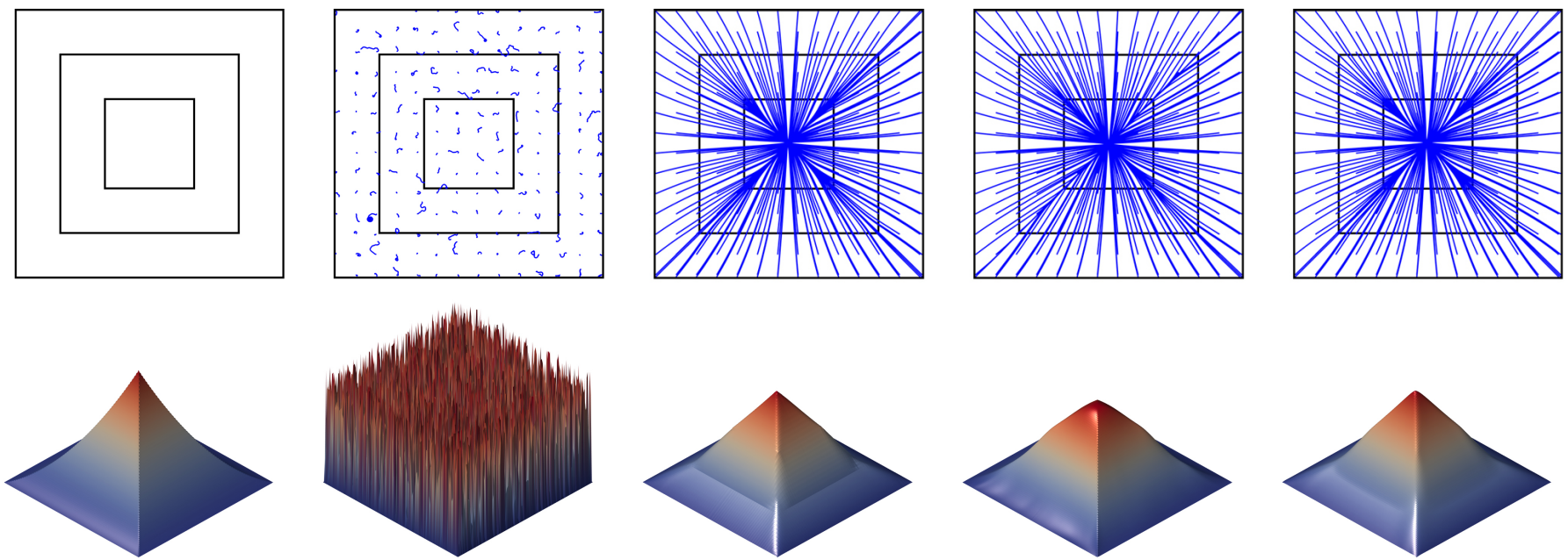

Ground Truth | Input | $\boldsymbol{\alpha} = (0, 1, 0)$ | $\boldsymbol{\alpha} = (0, 0, 1)$ | $\boldsymbol{\alpha} = (0, 1, 1)$

Pyramid results: 10 iterations. Parameters: $\eta = 100$, $\mu = \zeta = 1$.

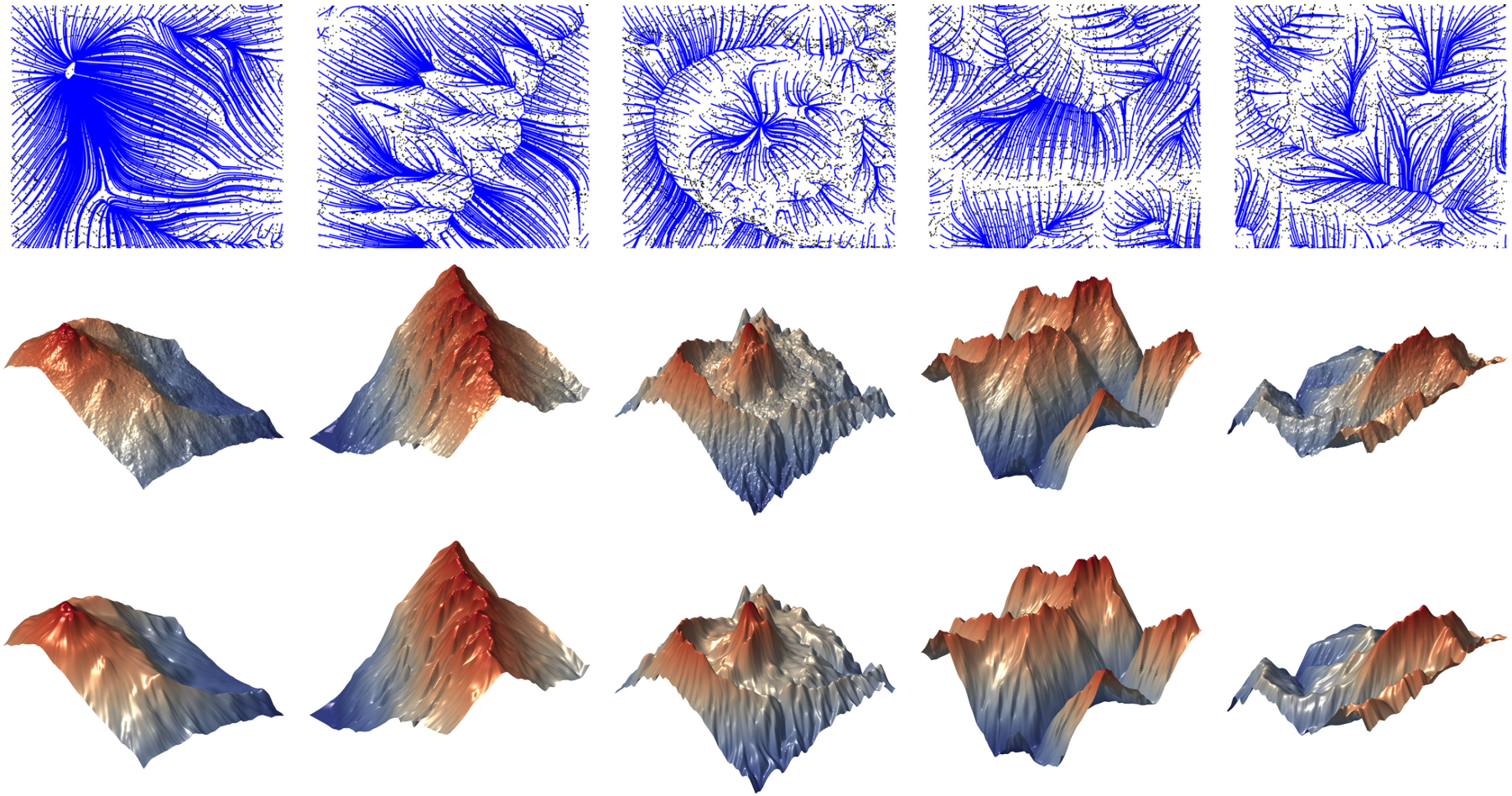

Etna Monte Baldo Vesuvio Vipiteno Gran Sasso

SRTM dataset (7% data). Streamlines (top), ground truth (middle), results (bottom).
Parameters: joint 2nd and 3rd orders, $\alpha_{2,0} = 0.1, \alpha_{3,0} = 1$, $\mu = \zeta = 1$, $\eta = 1000$.

TDV: Atomic Force Microscopy

Comparison with
(Oxvig, Arildsen, Larsen, 2017)

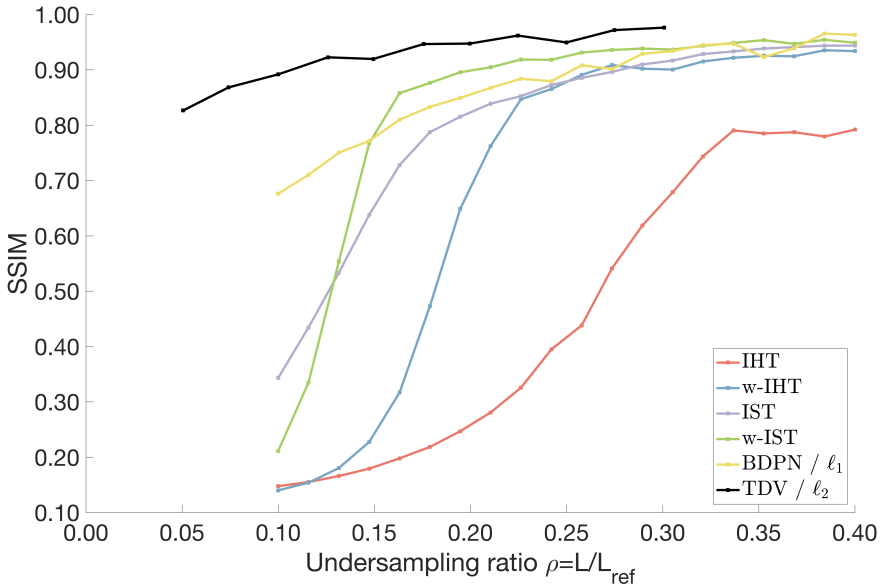

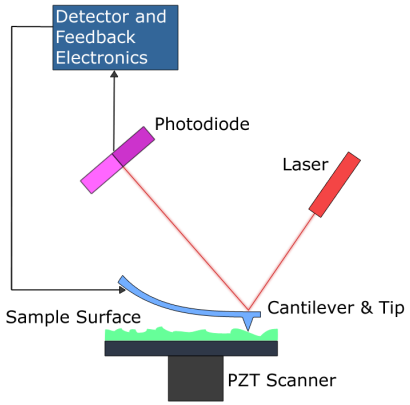

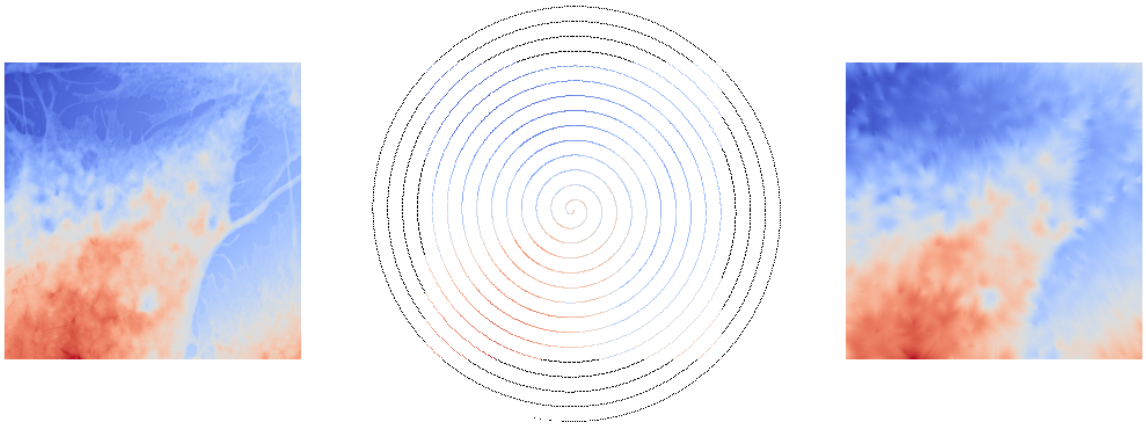

Ground Truth (left), Sampling (middle), Result (right). Percentage: 05.06%

TDV: video denoising

$$\mathrm{TDV}\,(u,\mathbf{M}) = \sup_{\boldsymbol{\Psi}} \left\{ \int_\Omega (\mathbf{M}\widetilde{\boldsymbol{\nabla}} \otimes u) \cdot \boldsymbol{\Psi}\, \mathrm{d}\boldsymbol{x} \;\middle|\; \text{for all suitable test functions } \boldsymbol{\Psi} \right\}.$$

$$\mathbf{M}\widetilde{\boldsymbol{\nabla}} \otimes u = \underbrace{\begin{pmatrix} a^{x,y} & 0 & 0 & 0 & 0 & 0 \\ 0 & 1 & 0 & 0 & 0 & 0 \\ 0 & 0 & a^{x,t} & 0 & 0 & 0 \\ 0 & 0 & 0 & 1 & 0 & 0 \\ 0 & 0 & 0 & 0 & a^{y,t} & 0 \\ 0 & 0 & 0 & 0 & 0 & 1 \end{pmatrix} \begin{pmatrix} e_{2,1} & e_{2,2} & 0 & 0 & 0 & 0 \\ e_{1,1} & e_{1,2} & 0 & 0 & 0 & 0 \\ 0 & 0 & e_{4,1} & e_{4,2} & 0 & 0 \\ 0 & 0 & e_{3,1} & e_{3,2} & 0 & 0 \\ 0 & 0 & 0 & 0 & e_{6,1} & e_{6,2} \\ 0 & 0 & 0 & 0 & e_{5,1} & e_{5,2} \end{pmatrix}}_{\mathbf{M}} \underbrace{\begin{pmatrix} \partial_x \\ \partial_y \\ \partial_x \\ \partial_t \\ \partial_y \\ \partial_t \end{pmatrix}}_{\widetilde{\boldsymbol{\nabla}}} \otimes u$$

$$= \left(a^{x,y}\, \boldsymbol{\nabla}^{x,y}_{\boldsymbol{e}_2} u, \quad \boldsymbol{\nabla}^{x,y}_{\boldsymbol{e}_1} u, \quad a^{x,t}\, \boldsymbol{\nabla}^{x,t}_{\boldsymbol{e}_4} u, \quad \boldsymbol{\nabla}^{x,t}_{\boldsymbol{e}_3} u, \quad a^{y,t}\, \boldsymbol{\nabla}^{y,t}_{\boldsymbol{e}_6} u, \quad \boldsymbol{\nabla}^{y,t}_{\boldsymbol{e}_5} u \right)^{\mathrm{T}}.$$

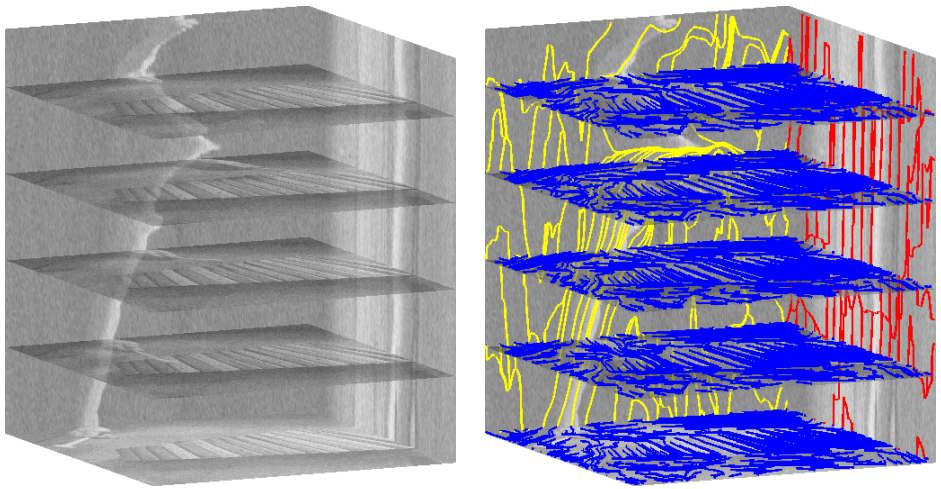

Left: `xylophone.mp4` (Gaussian noise $\varsigma = 20$); right: streamlines of $\boldsymbol{e}_1$ (blue), $\boldsymbol{e}_3$ (red) and $\boldsymbol{e}_5$ (yellow).

TDV: video denoising with linesearch parameters

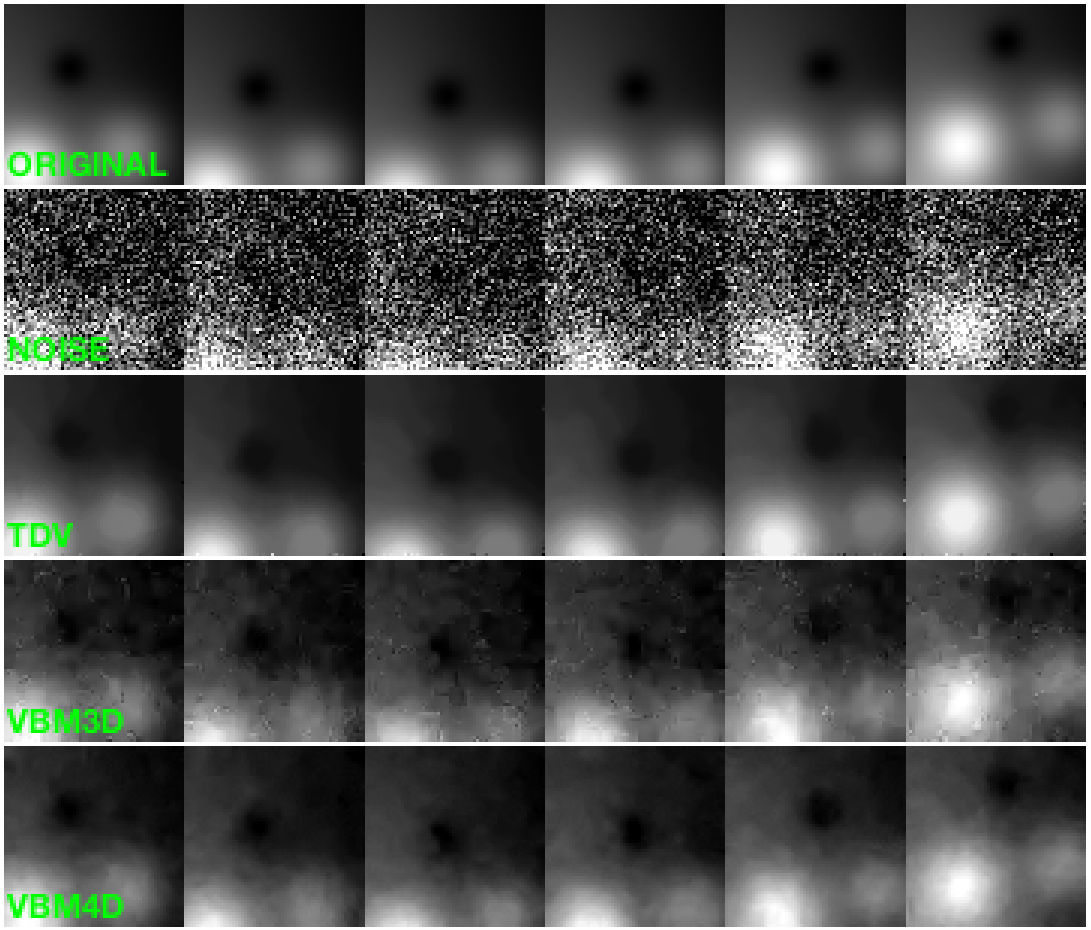

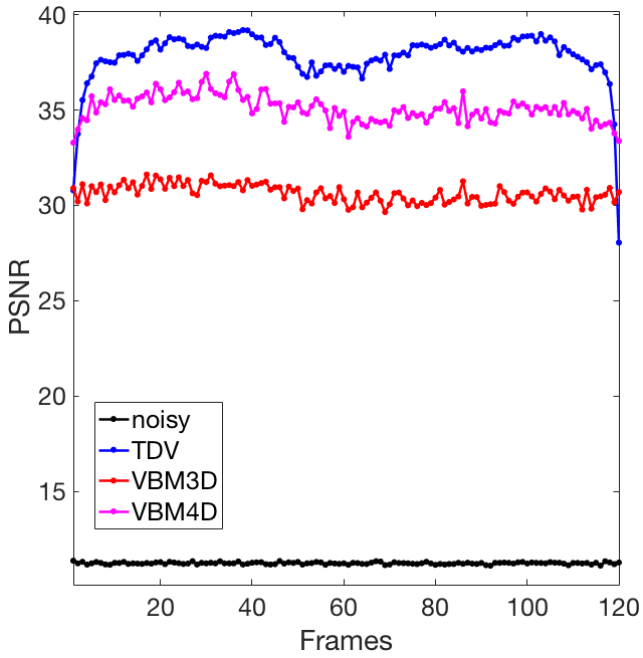

Franke: frames [10, 20, 30, 40, 50, 60],
Gaussian noise $\varsigma = 70$ (out of 255),
$\sigma = 3.00, \rho = 3.00, \eta = 02.45.$

TDV: video denoising without linesearch parameters

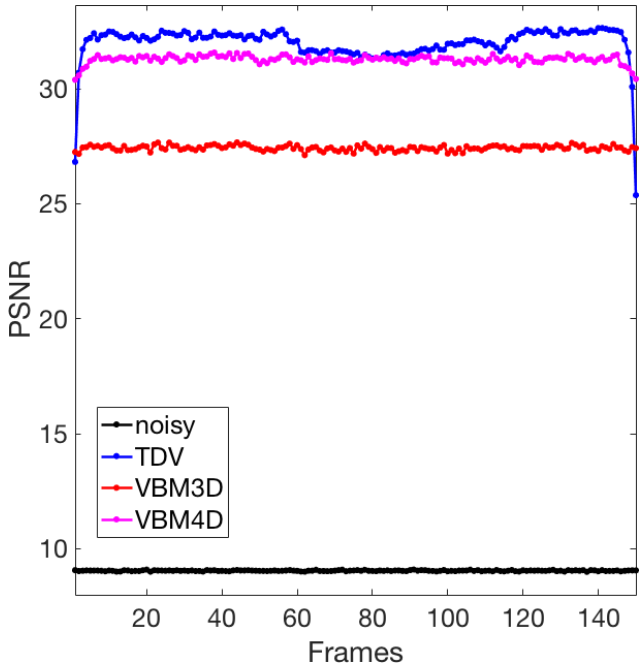

Miss America: frames [10, 20, 30, 40, 50, 60],
Gaussian noise $\varsigma = 90$ (out of 255),
$\sigma = \rho = 3.2\varsigma^{-0.5}, \eta = 255\varsigma^{-1}$.

Osmosis: standard filter

Weickert, Vogel, Setzer, Hagenburg, Breuß ('11-'13): given $v : \Omega \to \mathbb{R}$, find $u : \Omega \to \mathbb{R}$:

$$\min_u E^v(u), \quad E^v(u) := \int_\Omega v \left| \boldsymbol{\nabla} \left(\frac{u}{v} \right) \right|^2 \mathrm{d}\boldsymbol{x}.$$

For $\boldsymbol{d} = \boldsymbol{\nabla} \log v$ and $f : \Omega \to \mathbb{R}$, u is the **steady-state solution** of the drift-diffusion PDE:

$$\begin{cases} \partial_t u = \operatorname{div}(\boldsymbol{\nabla} u - \boldsymbol{d}u) = \Delta u - \operatorname{div}(\boldsymbol{d}u) & \text{on } \Omega \times (0, T], \\ u(\boldsymbol{x}, 0) = f(\boldsymbol{x}) & \text{on } \Omega, \\ \langle \boldsymbol{\nabla} u - \boldsymbol{d}u, \boldsymbol{n} \rangle = 0 & \text{on } \partial\Omega \times (0, T]. \end{cases}$$

v

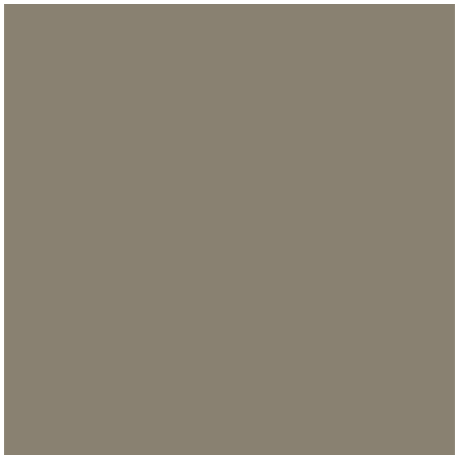

u^{t_0}

Osmosis: continuous and discrete setting

Continuous osmosis model

$$\begin{cases} \partial_t u = \operatorname{div}(\boldsymbol{\nabla} u - \boldsymbol{d}u) = \Delta u - \operatorname{div}(\boldsymbol{d}u) & \text{on } \Omega \times (0,T], \\ u(\boldsymbol{x},0) = f(\boldsymbol{x}) & \text{on } \Omega, \\ \langle\, \boldsymbol{\nabla} u - \boldsymbol{d}u, \boldsymbol{n} \,\rangle = 0 & \text{on } \partial\Omega \times (0,T]. \end{cases}$$

Continuous model (Proposition 1, Weickert et al., 2013)

The solution of the PDE osmosis model enjoys the following properties:

- **mass conservation (AVG)**: $\frac{1}{|\Omega|}\int_\Omega u(\boldsymbol{x},t)\,\mathrm{d}\boldsymbol{x} = \frac{1}{|\Omega|}\int_\Omega f(\boldsymbol{x})\,\mathrm{d}\boldsymbol{x}$ for all $t > 0$;
- **non-negativity**: $u(\boldsymbol{x},t) \geq 0$ for all $\boldsymbol{x} \in \Omega$ and $t > 0$ (osmosis may violate max-min);
- **non-constant steady states**: for $v > 0$, $\boldsymbol{d} := \boldsymbol{\nabla} \log v$, the stationary solution is:

$$w(\boldsymbol{x}) := \frac{\mu_f}{\mu_v} v(\boldsymbol{x}).$$

Valid also in the discrete for suitable space discretization $\mathbf{A}$ and Explicit/Implicit-Euler.

Spatial discretisation of osmosis (Vogel et al.,2013)

The FD spatial discretisation at $(x_i, y_j) = ((i-0.5)h, (j-0.5)h)$ is a 5 point stencil:

$$(\partial_t u)_{i,j} = (\mathbf{A}u)_{i,j}, \quad \text{with } \mathbf{A} \in \mathbb{R}^{MN \times MN}$$

$$\begin{aligned}\mathbf{A} := &\frac{u_{i+1,j} - 2u_{i,j} + u_{i-1,j}}{h^2} - \frac{1}{h}\left(d_{1,i+\frac{1}{2},j}\frac{u_{i+1,j}+u_{i,j}}{2} - d_{1,i-\frac{1}{2},j}\frac{u_{i,j}+u_{i-1,j}}{2}\right)\\ &+ \frac{u_{i,j+1} - 2u_{i,j} + u_{i,j-1}}{h^2} - \frac{1}{h}\left(d_{2,i,j+\frac{1}{2}}\frac{u_{i,j+1}+u_{i,j}}{2} - d_{2,i,j-\frac{1}{2}}\frac{u_{i,j}+u_{i,j-1}}{2}\right)\end{aligned}$$

$\mathbf{A}$ is irreducible (non-symm.), with zero-column sum and non-neg. off-diagonal entries.

Scale-space theory in Vogel et al. ('13)

Let $\mathbf{A}$ as above. For $k \geq 0$, the time-discretisation schemes for $\mathbf{P} \in \mathbb{R}^{MN \times MN}$ is:

$$\begin{cases} u^0 = f & \text{if } k = 0, \\ u^{k+1} = \mathbf{P}u^k & \text{if } k \geq 1. \end{cases}$$

Then $\mathbf{P}$ is the (non-symmetric) irreducible, non-negative matrix with strictly positive diagonal entries and unitary column sum such that

1. the evolution preserves **positivity** and the **average grey value** of f;
2. the eigenvector of $\mathbf{P}$ with eigenvalue 1 is the **unique steady state** for $k \to \infty$.

Osmosis: dimensional splitting

We focus on **dimensional splitting** $\mathbf{A_{full}} := \mathbf{A_1} + \mathbf{A_2}$ for **large** images.

$$\mathbf{A_1}(\boldsymbol{u}) := \frac{u_{i+1,j} - 2u_{i,j} + u_{i-1,j}}{h^2} - \frac{1}{h}\left(d_{1,i+\frac{1}{2},j}\frac{u_{i+1,j}+u_{i,j}}{2} - d_{1,i-\frac{1}{2},j}\frac{u_{i,j}+u_{i-1,j}}{2}\right)$$

$$\mathbf{A_2}(\boldsymbol{u}) := \frac{u_{i,j+1} - 2u_{i,j} + u_{i,j-1}}{h^2} - \frac{1}{h}\left(d_{2,i,j+\frac{1}{2}}\frac{u_{i,j+1}+u_{i,j}}{2} - d_{2,i,j-\frac{1}{2}}\frac{u_{i,j}+u_{i,j-1}}{2}\right)$$

Method	$\mathbf{P}$	$\tau <$ step-size limitation	AVG	pos.	conv.
E. Euler	$\mathbf{P}^{+}_{\mathbf{full},\tau} = (\mathbf{I} + \tau\mathbf{A_{full}})$	$\left(\max_i \left\lvert(\mathbf{A_{full}})_{i,i}\right\rvert\right)^{-1}$	✓	✓	✓
I. Euler	$\mathbf{P}^{-}_{\mathbf{full},\tau} = (\mathbf{I} - \tau\mathbf{A_{full}})^{-1}$	no	✓	✓	✓
P.R.	$\mathbf{P}^{-}_{\mathbf{1},\frac{\tau}{2}}\mathbf{P}^{+}_{\mathbf{2},\frac{\tau}{2}}\mathbf{P}^{-}_{\mathbf{2},\frac{\tau}{2}}\mathbf{P}^{+}_{\mathbf{1},\frac{\tau}{2}}$,	$2\left(\max_{\boldsymbol{n}}\max_i \left\lvert(\mathbf{A}_{\boldsymbol{n}})_{i,i}\right\rvert\right)^{-1}$	✓	✓	✓
Douglas	$\mathbf{I} + \tau\mathbf{P}^{-}_{\mathbf{2},\theta\tau}\mathbf{P}^{-}_{\mathbf{1},\theta\tau}\mathbf{A_{full}}$	$\left(\max_i \left\lvert\mathbf{P}^{-}_{\mathbf{2},\theta\tau}\mathbf{P}^{-}_{\mathbf{1},\theta\tau}\mathbf{A_{full}}\right\rvert_{i,i}\right)^{-1}$	✓	?	?
AOS	$\frac{1}{2}\sum_{\boldsymbol{n}=1}^{2}\mathbf{P}^{-}_{\boldsymbol{n},2\tau}$	no	✓	✓	✓
MOS	$\prod_{\boldsymbol{n}=1}^{2}\mathbf{P}^{-}_{\boldsymbol{n},\tau}$	no	✓	✓	✓
AMOS	$\frac{1}{2}\sum_{\substack{\boldsymbol{n}=1\\ \boldsymbol{i}=\{1,2\}\\ \boldsymbol{j}=\{2,1\}}}^{2}\mathbf{P}^{-}_{\boldsymbol{j_n},\tau}\mathbf{P}^{-}_{\boldsymbol{i_n},\tau}$	no	✓	✓	✓

Osmosis: the integrable case

P.R.

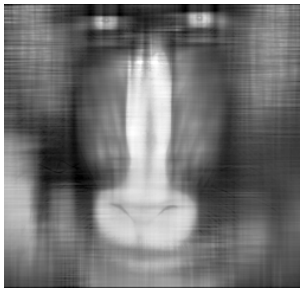

Douglas, $\theta = 1$.

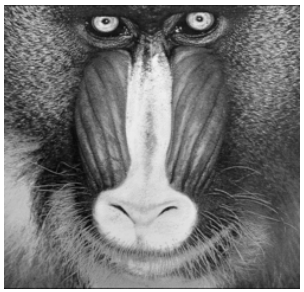

AOS.

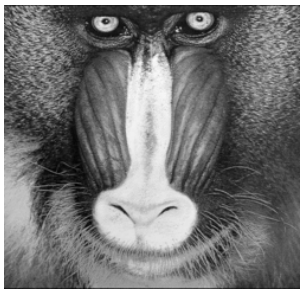

MOS.

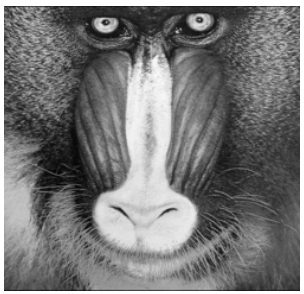

AMOS.

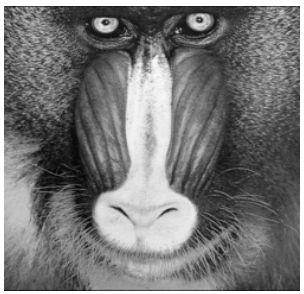

LU, $\theta = 1$.

Params.: $\tau = 1000$, $T = 5000$

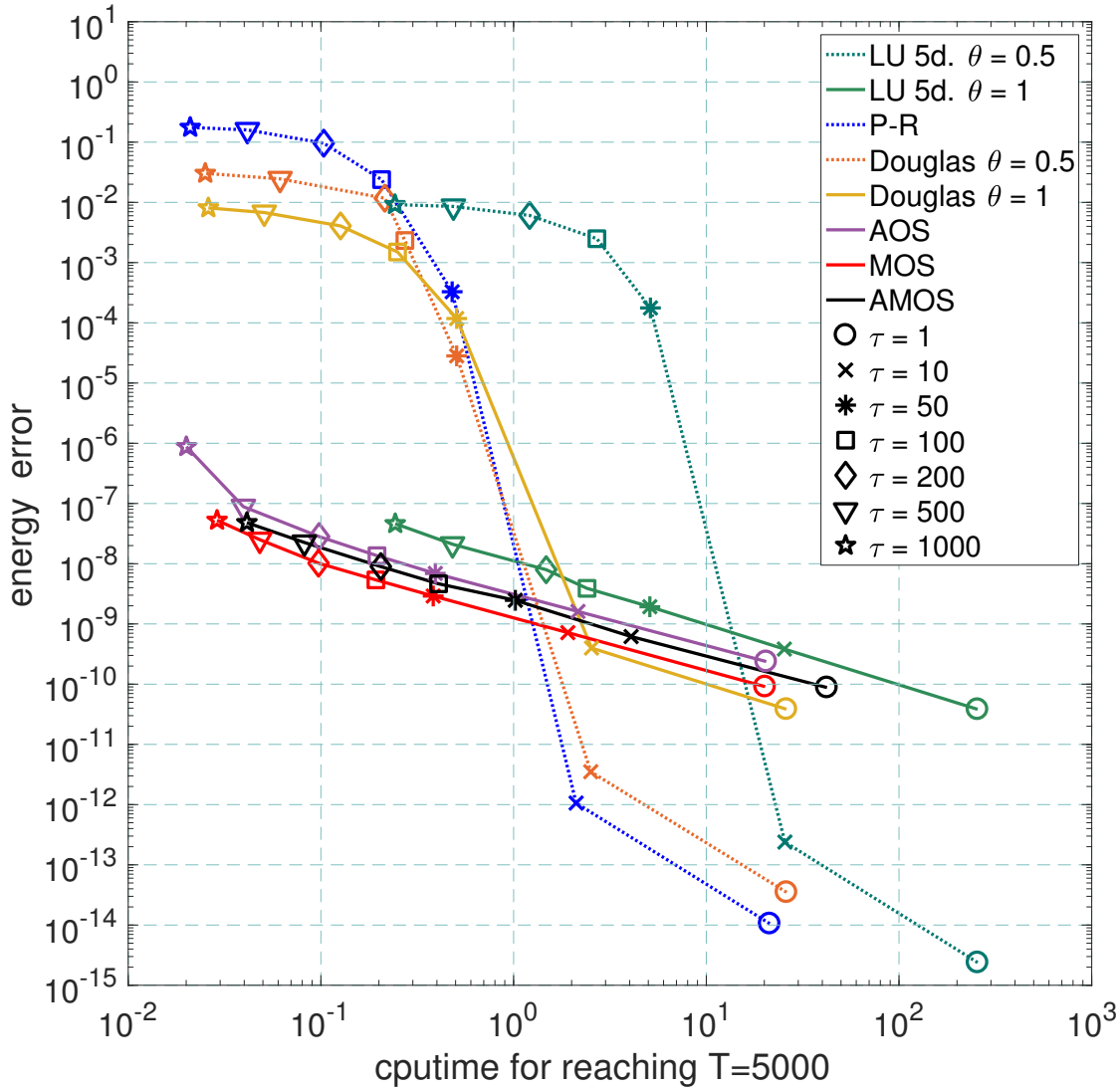

Osmosis: the fully non-integrable case

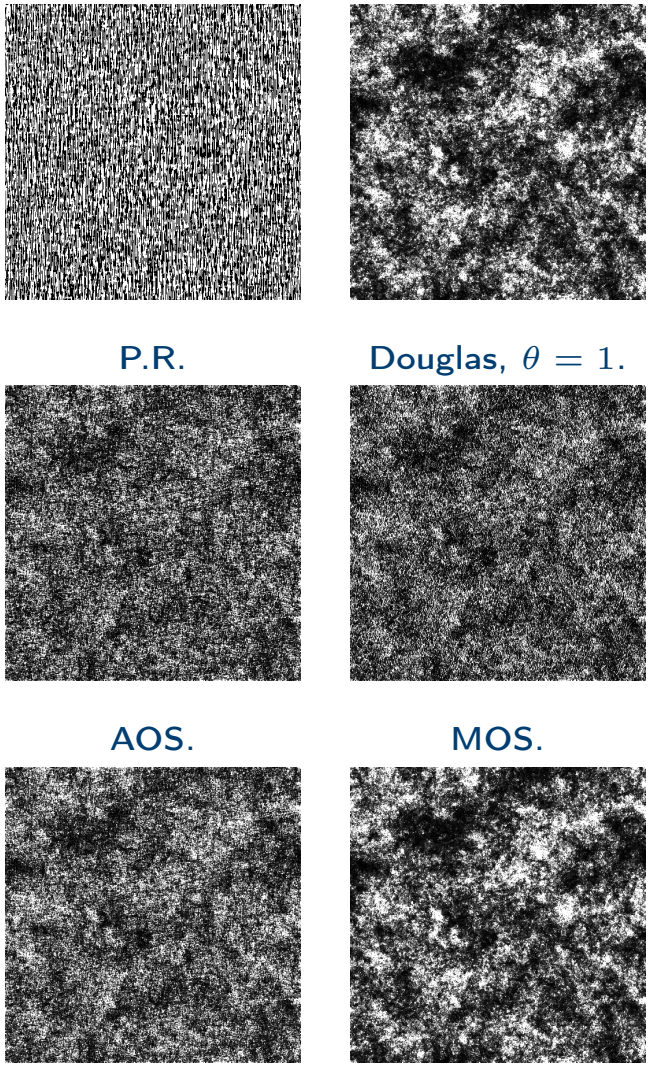

P.R. Douglas, $\theta = 1$.

AOS. MOS.

AMOS. Expl., $\tau = 0.12$.

Params: $\tau = 25$ (but Expl.), $T = 3000$

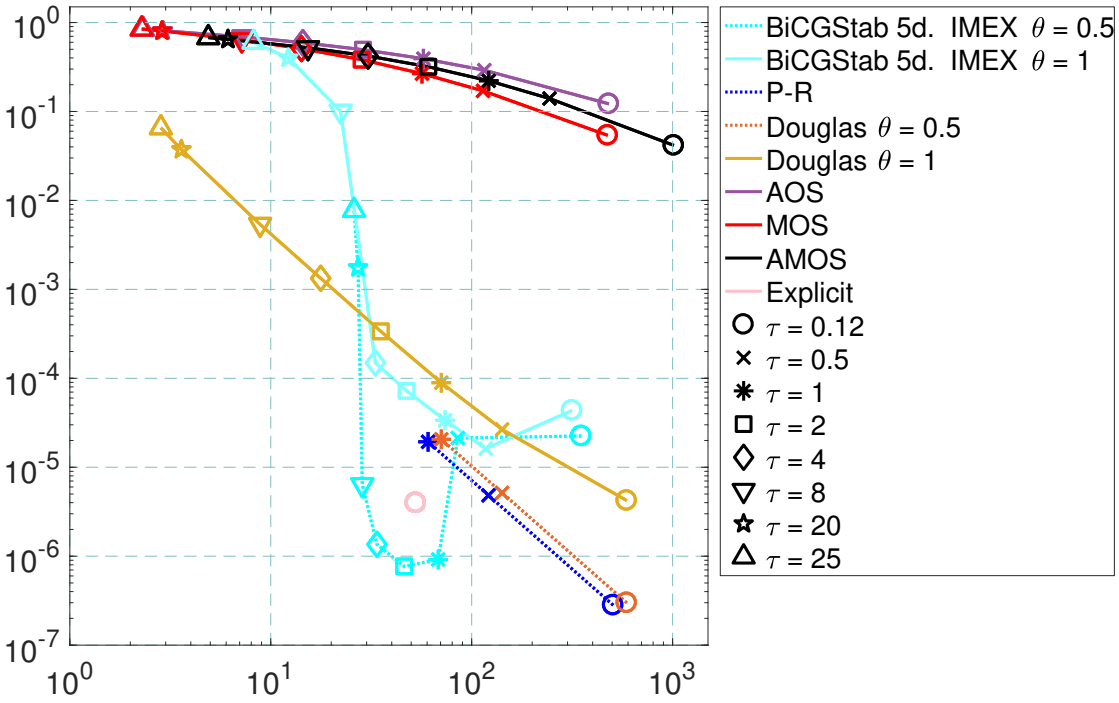

cputime (x-axis) vs. rRMSE (y-axis) for $T = 3000$ (avg. of 10 tests).

Osmosis: the shadow removal problem

Good news: we can modify (slightly) the vector field $\boldsymbol{d}$ for other imaging applications.

Let $f \equiv v : \Omega \to \mathbb{R}^+$ be a image corrupted by a **constant** shadow, $\Omega = \Omega_{\text{out}} \cup \Omega_{\text{sb}} \cup \Omega_{\text{in}}$.

Decomposition of a shadowed image into Ω_{out}, Ω_{sb} and Ω_{in}.

Shadow removal problem via osmosis: recover the correct light coefficient

$$\begin{cases} \partial_t u = \Delta u - \operatorname{div}(\boldsymbol{d}u) & \text{on } \Omega_{\text{in}} \cup \Omega_{\text{out}} \times (0,T], \\ \partial_t u = \Delta u & \text{on } \Omega_{\text{sb}} \times (0,T], \\ u(\boldsymbol{x},0) = f(\boldsymbol{x}) & \text{on } \Omega, \\ \langle \boldsymbol{\nabla} u - \boldsymbol{d}u, \boldsymbol{n} \rangle = 0 & \text{on } \partial\Omega \times (0,T]. \end{cases} \quad \text{where} \quad \boldsymbol{d} := \begin{cases} \boldsymbol{\nabla} \log f & \text{on } \Omega_{\text{in}} \cup \Omega_{\text{out}}, \\ 0 & \text{on } \Omega_{\text{sb}}. \end{cases}$$

Osmosis acts as inpainting on Ω_{sb}: Δu **diffuses** the structures **isotropically** and **smoothly**.

Possible solution: **post-processing** inpainting step (Arias, Facciolo, Caselles & Sapiro, 2011)

Shadowed

Boundary

Standard osmosis

Inpainted

Standard osmosis (zoom)

Inpainted (zoom)

Osmosis: anisotropic generalisation

Aim: do shadow removal and inpainting **jointly** to avoid the blurring artefact.

from *standard osmosis energy* to *anisotropic osmosis energy*

$$\text{from} \quad E^v(u) := \int_\Omega v \left| \nabla \left(\frac{u}{v} \right) \right|^2 \mathrm{d}\boldsymbol{x} \quad \text{to} \quad E^v_{\boldsymbol{b},\theta}(u) := \int_\Omega v \left| \mathbf{M}_{\boldsymbol{b},\theta} \nabla \left(\frac{u}{v} \right) \right|^2 \mathrm{d}\boldsymbol{x}.$$

$$E_{\boldsymbol{b},\theta}(u) := \int_\Omega v \left\langle \mathbf{W}_{\boldsymbol{b},\theta} \nabla \left(\frac{u}{v} \right), \nabla \left(\frac{u}{v} \right) \right\rangle \mathrm{d}\boldsymbol{x}, \quad \text{where } \mathbf{W}_{\boldsymbol{b},\theta} = b_1^2(\boldsymbol{z} \otimes \boldsymbol{z}) + b_2^2(\boldsymbol{z}^\perp \otimes \boldsymbol{z}^\perp).$$

from *standard osmosis PDE* to *anisotropic osmosis PDE*

$$\text{from} \quad \begin{cases} \partial_t u = \operatorname{div}(\nabla u - \boldsymbol{d}u) \\ u(\boldsymbol{x}, 0) = f(\boldsymbol{x}) \\ \langle \nabla u - \boldsymbol{d}u, \boldsymbol{n} \rangle = 0 \end{cases} \quad \text{to} \quad \begin{cases} \partial_t u = \operatorname{div}\left(\mathbf{W}_{\boldsymbol{b},\theta}(\nabla u - \boldsymbol{d}u)\right) & \text{on } \Omega \times (0,T], \\ u(\boldsymbol{x}, 0) = f(\boldsymbol{x}) & \text{on } \Omega \\ \langle \mathbf{W}_{\boldsymbol{b},\theta}(\nabla u - \boldsymbol{d}u), \boldsymbol{n} \rangle = 0 & \text{on } \partial\Omega \times (0,T]. \end{cases}$$

- conservation of **mass** (AVG);
- conservation of **non-negativity**;
- convergence to **non-constant steady states**.

Osmosis: anisotropic shadow removal, numerical details

Anisotropic osmosis for shadow removal: standard on $\Omega \setminus \Omega_{\text{sb}}$, directional on Ω_{sb}

$$\begin{cases} \partial_t u = \operatorname{div}\left(\mathbf{W}_{\boldsymbol{b},\boldsymbol{z}}(\boldsymbol{\nabla} u - \boldsymbol{d}u)\right) & \text{on } \Omega \times (0,T], \\ u(\boldsymbol{x},0) = f(\boldsymbol{x}) & \text{on } \Omega, \\ \langle\, \mathbf{W}_{\boldsymbol{b},\boldsymbol{z}}\,(\boldsymbol{\nabla} u - \boldsymbol{d}u)\,, \boldsymbol{n}\,\rangle = 0 & \text{on } \partial\Omega \times (0,T], \end{cases}$$

$$\boldsymbol{d}(\boldsymbol{x}) = \begin{cases} \boldsymbol{\nabla} \log f, & \text{if} \quad \boldsymbol{x} \in \Omega \setminus \Omega_{\text{sb}}, \\ 0, & \text{if} \quad \boldsymbol{x} \in \Omega_{\text{sb}}. \end{cases} \quad \text{and} \quad \boldsymbol{b}(\boldsymbol{x}) = \begin{cases} (1,1), & \text{if} \quad \boldsymbol{x} \in \Omega \setminus \Omega_{\text{sb}}, \\ (0,1), & \text{if} \quad \boldsymbol{x} \in \Omega_{\text{sb}}. \end{cases}$$

Space discretisation for $\mathbf{A}$

- AD-LBR, Fehrenbach & Mirebeau ('13): sparse (6d) non-neg., oriented as $\mathbf{W}_{\boldsymbol{b},\theta}$.

Time solver: exponential integrators for exact-in-time solution at T

$$u^T = \exp(\tau \mathbf{A}) u^0, \quad \text{with } \tau := T - t_0.$$

- we approximate $\exp(\tau A)u^0$ via Leja interpolation as in Caliari et al. ('16);
- **scale-space properties are preserved** by exponential integrators provided good $\mathbf{A}$;

Osmosis: anisotropic shadow removal on synthetic images

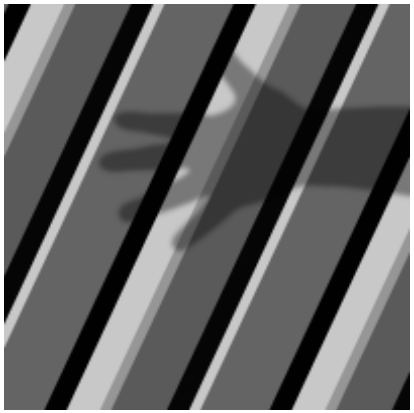

Shadowed f

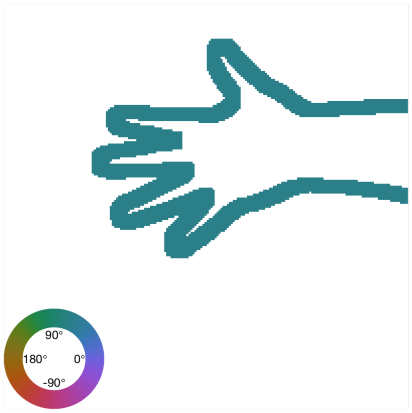

Orientation angle θ

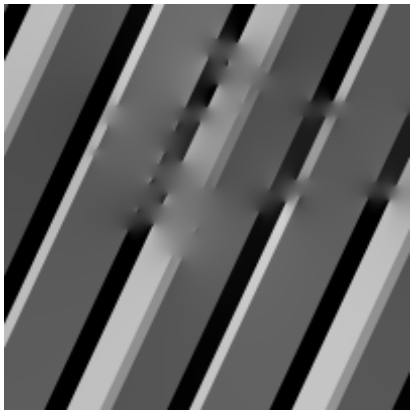

Isotropic osmosis

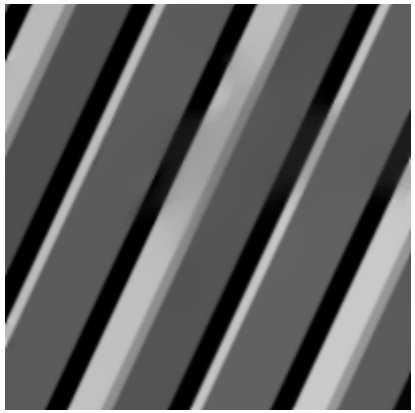

Anisotropic osmosis

Shadowed f

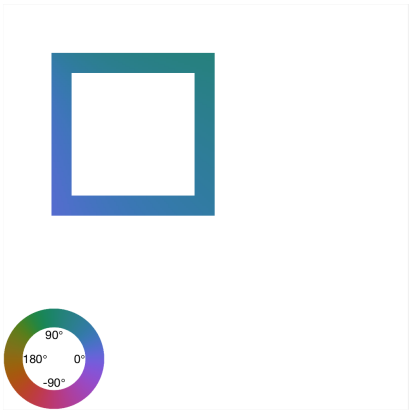

Orientation angle θ

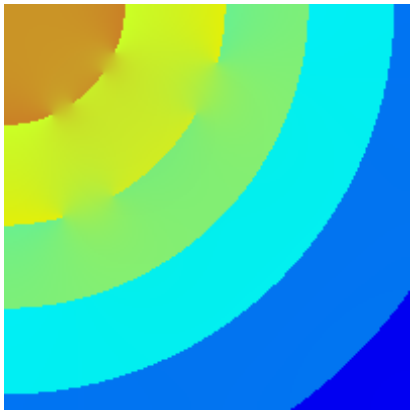

Isotropic osmosis

Anisotropic osmosis

Parameters: time step size $\tau = 100$, final time $T = 10000$, and smaller eigenvalue $\varepsilon = 0.05$.

Osmosis: estimation of directions in shadowed image

Let $\mathbf{A}$ be a 2-tensor on $\mathbb{R}^2$, decomposed as

$$\mathbf{A} = \underbrace{(\lambda_1 - \lambda_2)}_{\text{saliency}}(\boldsymbol{e}_1 \otimes \boldsymbol{e}_1) + \underbrace{\lambda_2}_{\text{ballness}}(\boldsymbol{e}_1 \otimes \boldsymbol{e}_1 + \boldsymbol{e}_2 \otimes \boldsymbol{e}_2)$$

- θ is the **orientation** (angle) formed by $\boldsymbol{e}_1$.

Tensor voting framework (TVF): Guy and Medioni ('96)

- neighbourhoods **vote for the most likely structure** (scale-depending);
- **efficiently** implemented by steerable filters in Franken et al. ('06);
- improves the structure tensor $K_\rho * (\boldsymbol{\nabla} u_\sigma \otimes \boldsymbol{\nabla} u_\sigma)$, see Moreno et al. ('12).

Proposed estimation: shadow boundary directions are biased:

1. **estimate** saliency and orientation θ from shadowed u;
2. **modify**: saliency=0 and θ randomized on shadow boundaries Ω_{sb};
3. **perform** tensor voting with **multi-scale** inspection.

Input

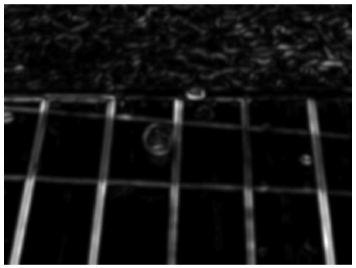

STF, λ_1

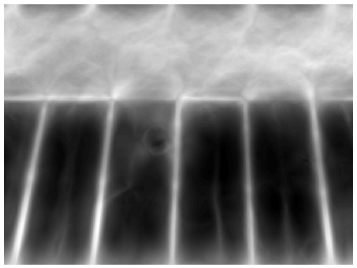

(mod.) TVF, λ_1

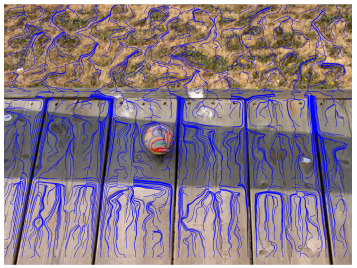

STF, e_1

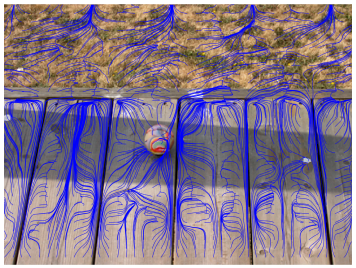

(mod.) TVF, e_1

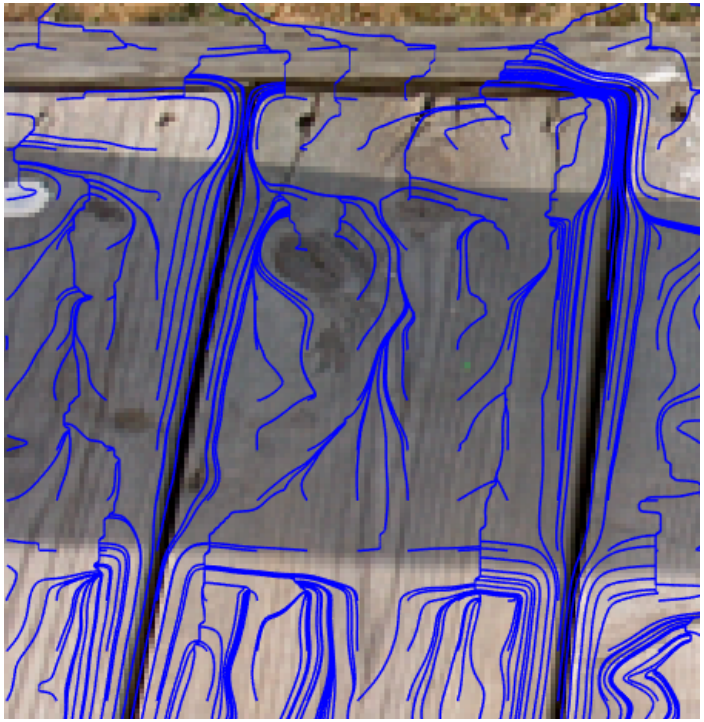

STF, e_1 (zoom)

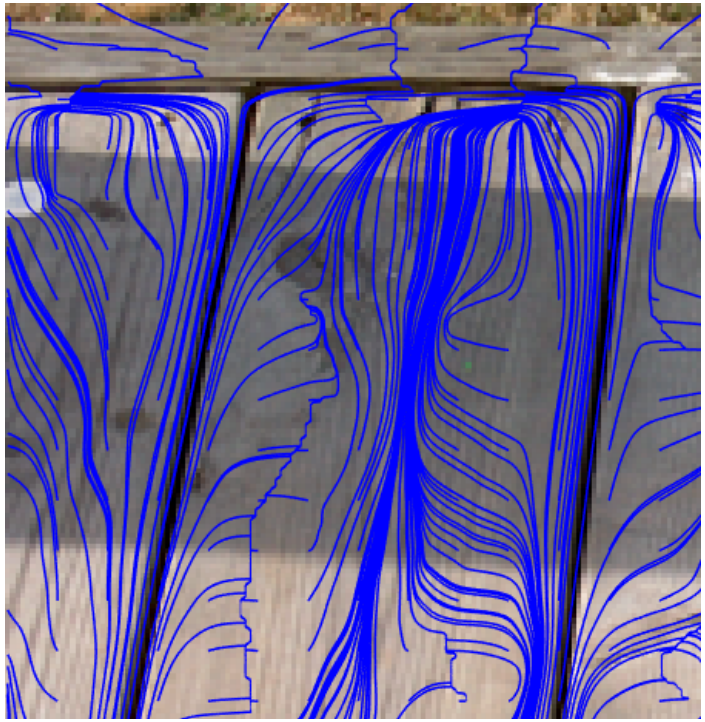

(mod.) TVF, e_1 (zoom)

Comparison: structure tensor (STF) with $(\sigma, \rho) = (2, 2)$ and tensor voting (TVF) with multi-scale $(11, 21, 31)$.

Osmosis: anisotropic shadow removal on real images

Shadowed f

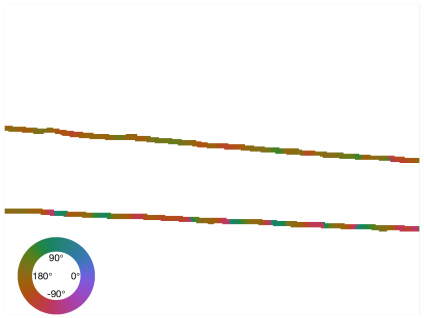

$\Omega_{\mathbf{sb}}$, θ for e_1

Isotropic osmosis

Anisotropic osmosis

Isotropic osmosis (zoom)

Anisotropic osmosis (zoom)

Parameters: $\boldsymbol{b} = (0.05, 1.00)$, $T = 1\text{e}5$, $\tau = 1\text{e}2$.

Osmosis: anisotropic shadow removal on real images

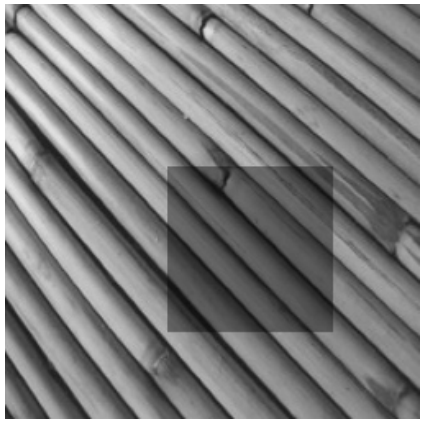

Shadowed f

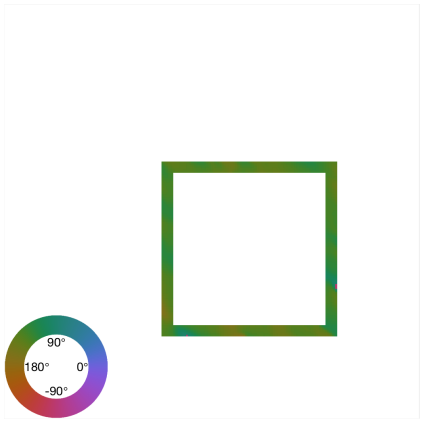

$\Omega_{\mathbf{sb}}$, θ for e_1

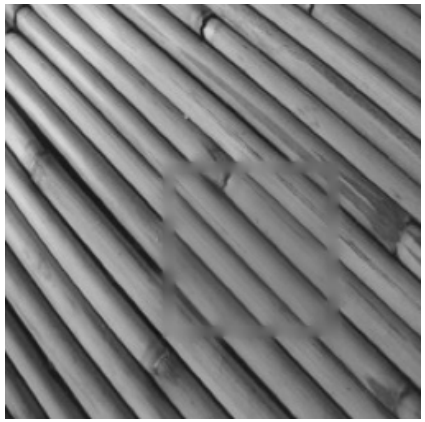

Isotropic osmosis

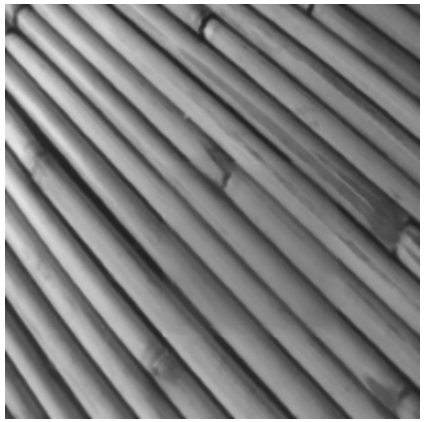

Anisotropic osmosis

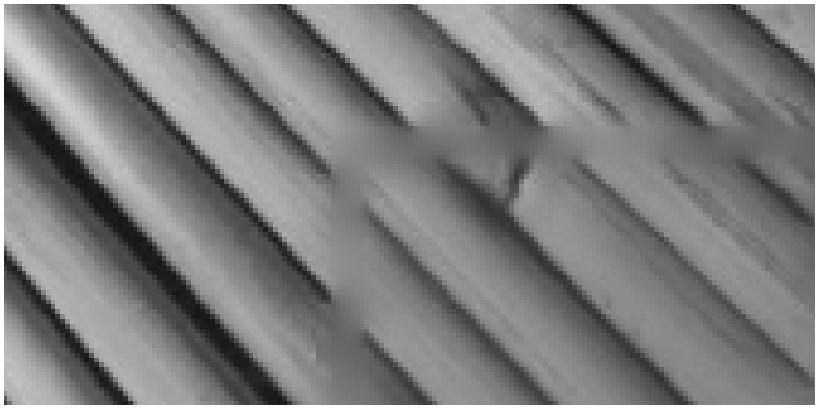

Isotropic osmosis (zoom)

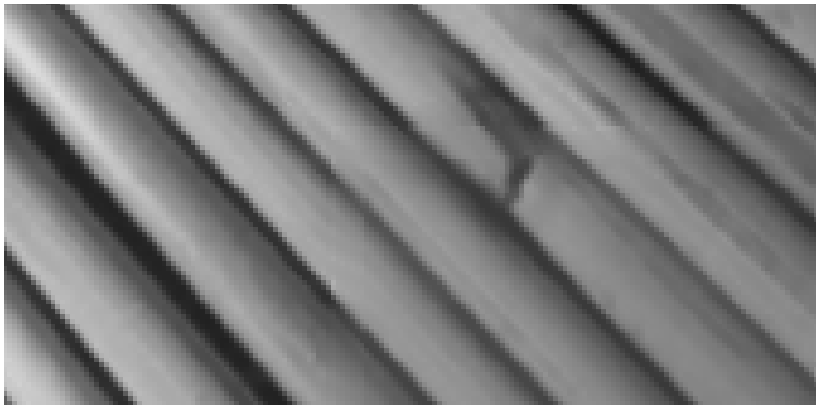

Anisotropic osmosis (zoom)

Parameters: $\boldsymbol{b} = (0.05, 1.00)$, $T = 1\text{e}5$, $\tau = 1\text{e}2$.

Osmosis: anisotropic shadow removal on real images

Shadowed f

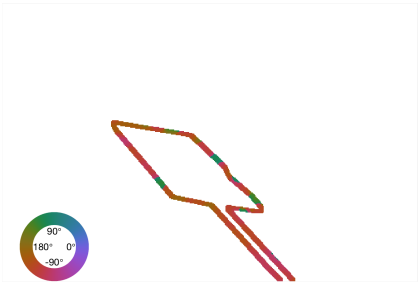

$\Omega_{\mathbf{sb}}$, θ for e_1

Isotropic osmosis

Anisotropic osmosis

Isotropic osmosis (zoom)

Anisotropic osmosis (zoom)

Parameters: $\boldsymbol{b} = (0.05, 1.00)$, $T = 1\text{e}5$, $\tau = 1\text{e}2$.

CH: "Monocromo" by Leonardo Da Vinci (fresco)

- **Sala delle Asse** (meaning *rooms of wooden planks*), Castello Sforzesco, Milan, Italy;
- 1498, **Ludovico Sforza** (*il Moro*) called **Leonardo** in Milan to depict the room;
- original destination: welcoming ambassadors;
- large **frescoes** (arbor's branches, mulberries,...) with monochrome technique;
- unfinished work (maybe with workshop);
- the room was turned into **barrack** and **stable**: **damaged** multiple times.

Left fresco

Central fresco

Sala delle Asse, Milan

Aim: **non-invasive mapping** of sub-superficial **defects** with sub-millimetric precision.

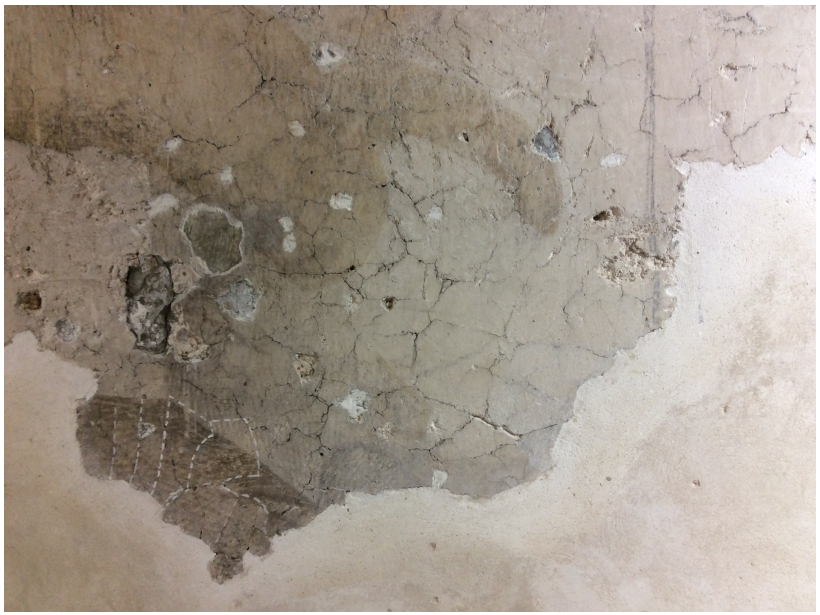

Wall damages

Sub-superficial holes

Approach: **dual-mode infrared** imaging (in collaboration with **Opificio delle Pietre Dure**)

CH: MWIR dual mode defect detection in frescoes

- **Reflection** mode: detect TQR radiation ρ in MWIR (only about 1% is emitted);
- **Emission** mode: insert $\varepsilon = 1 - \rho$ in recorded cooling-down thermograms.

Visible

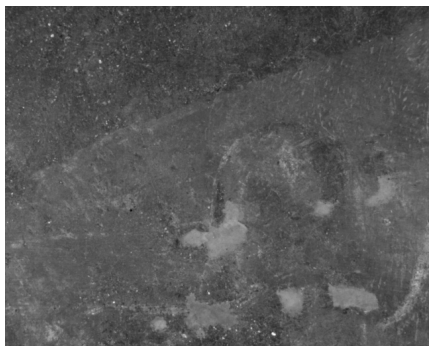

Reflectance
(TQR, registered)

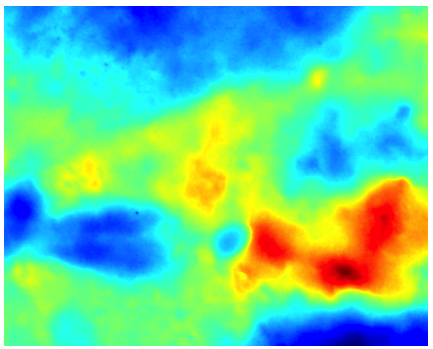

Thermogram
(ε-corrected, registered)

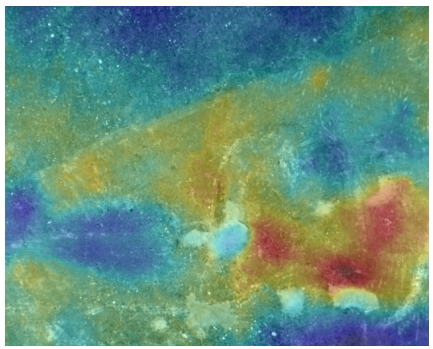

Super-imposition
Visible - IR Emission

CH: validation by experts

Discovering hidden features.

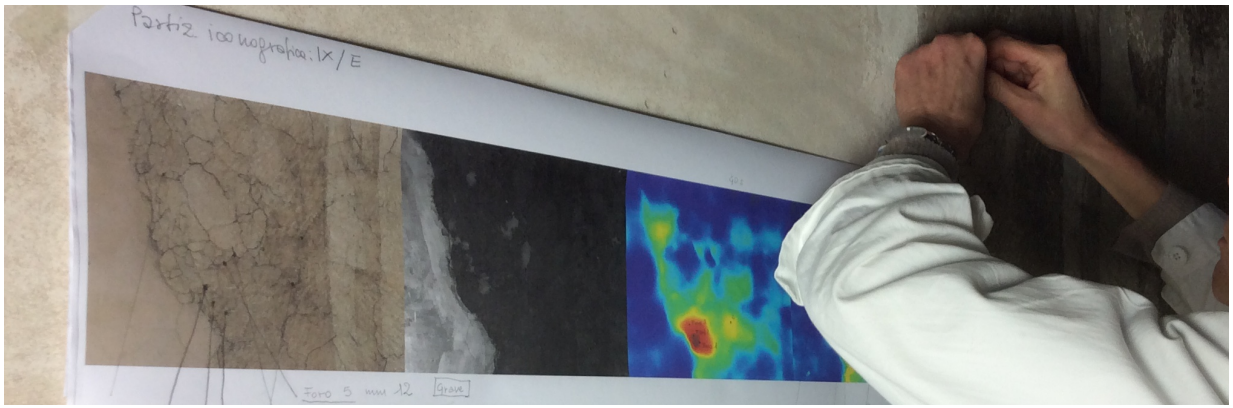

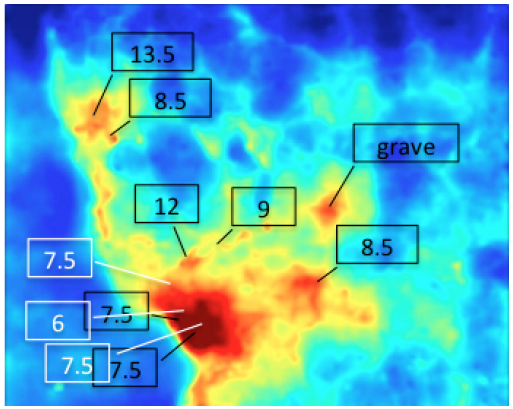

Measuring the defects (in mm) via the pin test (below) by experts of Opificio.

CH: TQR light balancing via efficient standard osmosis

How to **cover large walls**? Just **repeat** dual mode imaging and **mosaic**!

- **measurement errors**: due to moving the lighting setup (limited scaffolding space,. . .)
- errors seen as **inter-frame contrast change**: a lighting balance problem.

Visible (3 tiles)

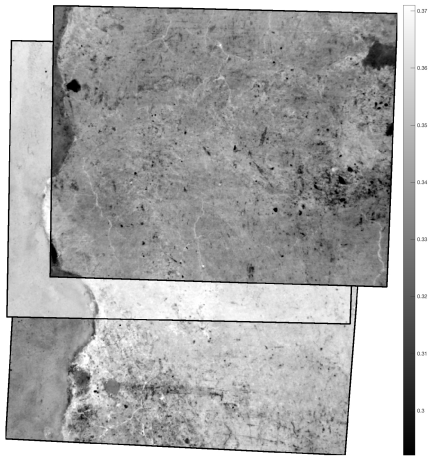

Emissivity from TQR

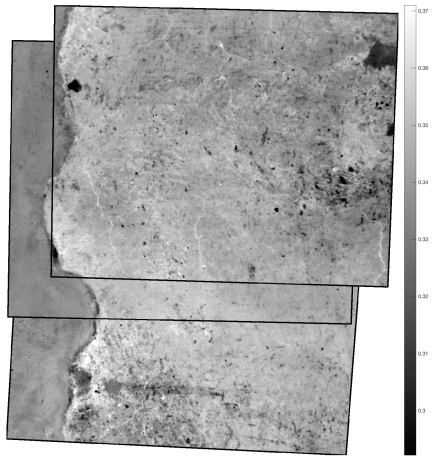

Corrected emissivity (via *osmosis*)

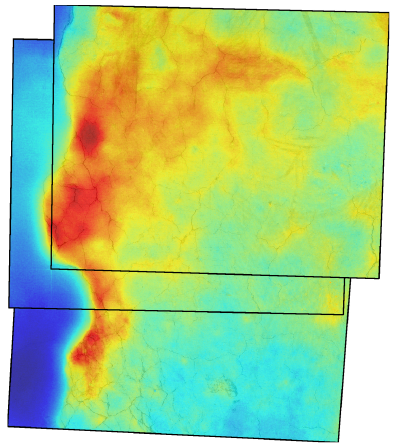

IR emission corrected with ε

CH: TQR light balancing via efficient standard osmosis

Monocromo, L. da Vinci

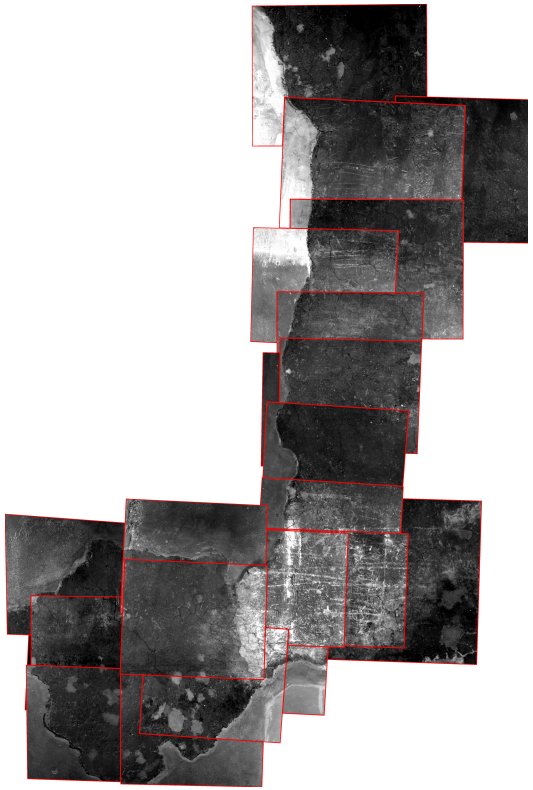

Shadowed ρ with red mask
33 TQR tiles (28 Megapixels)

Result $\tau = 1000$, $T = 100000$
(MOS 629 s., `BiCGStab` 4H)

CH: data fusion via efficient standard osmosis

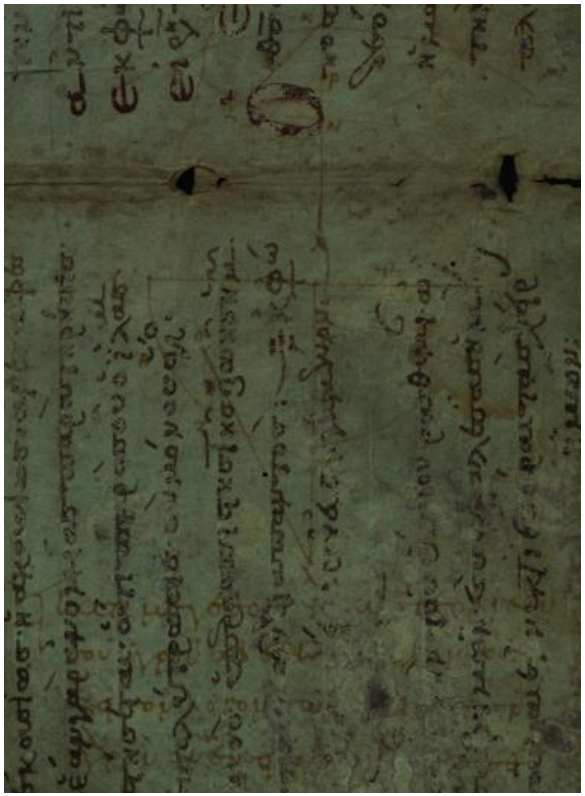

Original parchment (2MB) (zoom)

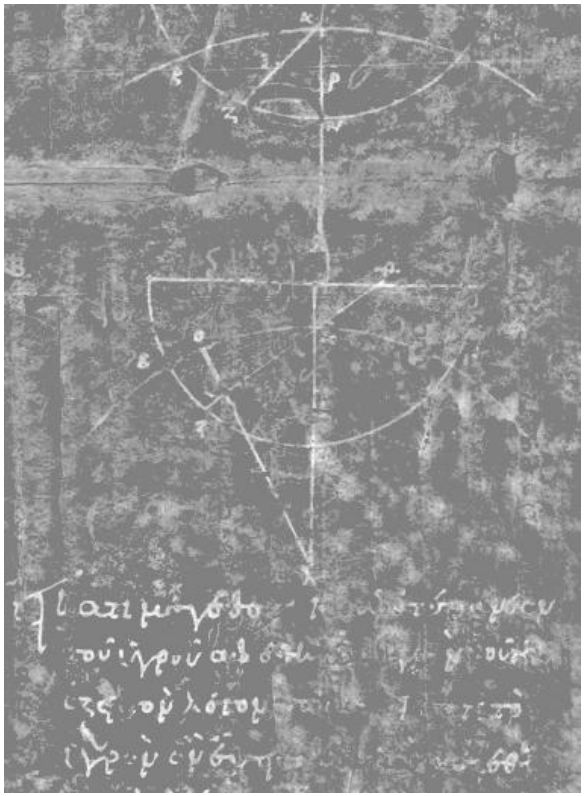

v with local Otsu (zoom)

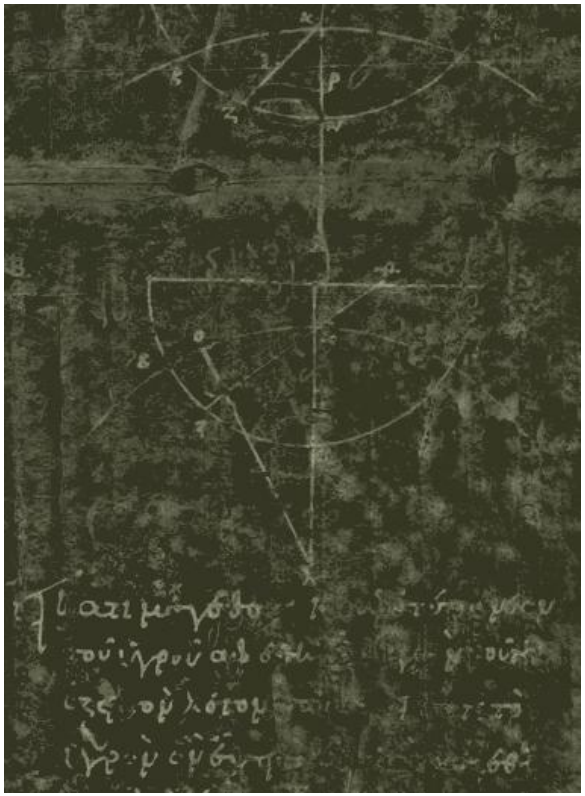

Result (MOS 137 s.) (zoom)

Archimedes palimpsest. X century copy of the works of Archimedes, overwritten in XIII century.

CH: restoration of manuscripts from Fitzwilliam Museum

Input

User selection

Chan-Vese segmentation

K-means segmentation

TV inpainting

Exemplar inpainting (5x5)

Relevant publications and pre-prints

- Parisotto, Lellmann, Masnou, Schönlieb. Higher-Order Total Directional Variation. Part I: Imaging Applications. arXiv:1812.05023 (2018)
- Parisotto, Masnou, Schönlieb. Higher-Order Total Directional Variation. Part II: Analysis. arXiv:1812.05061 (2018)
- Parisotto, Schönlieb. Total Directional Variation for Video Denoising. arXiv:1812.05063 (2018)
- Calatroni, Estatico, Garibaldi, Parisotto. Alternating Direction Implicit (ADI) schemes for a PDE-based image osmosis model. Journal of Physics: Conference Series 904 (1), 012014 (2015)
- Parisotto, Calatroni, Daffara. Digital Cultural Heritage Imaging via Osmosis Filtering. ICISP 2018. LNCS vol 10884, Springer (2018)
- Parisotto, Calatroni, Caliari, Schönlieb, Weickert. Anisotropic osmosis filtering for shadow removal in images. arXiv:1809.06298 (2018)
- Daffara, Parisotto, Mariotti. Mid-infrared thermal imaging for an effective mapping of surface materials and sub-surface detachments in mural paintings: integration of thermography and thermal quasi-reflectography. Optics for Arts, Architecture, and Archaeology V; 95270I (2015)
- Daffara, Parisotto, Ambrosini. Multipurpose, dual-mode imaging in the 3 µm to 5 µm range (MWIR) for artwork diagnostics: A systematic approach. Optics and Laser in Engineering, Vol. 104 (2018)
- Calatroni, d'Autume, Hocking, Panayotova, Parisotto, Ricciardi, Schönlieb. Unveiling the invisible: mathematical methods for restoring and interpreting illuminated manuscripts. Heritage Science 6:56, Springer (2018)

Thank you for your attention!